Iranian Journal of Science & Technology, Transaction B, Engineering, Vol. 31, No. B1, pp 49-63
Printed in The Islamic Republic of Iran, 2007

EFFECTS OF PLUNGING MOTION ON UNSTEADY AERODYNAMIC BEHAVIOR OF AN AIRCRAFT MODEL IN COMPRESSIBLE FLOW*

A. R. DAVARI AND M. R. SOLTANI**

Dept. of Engineering, Science and Research Campus, Azad University, I. R. of Iran
Email: msoltani@sharif.edu
Dept. of Aerospace Engineering, Sharif University of Technology, I. R. of Iran

Abstract– Aspects of pitching and plunging motions on unsteady aerodynamic behavior of an aircraft model were studied. Extensive wind tunnel tests were performed on a standard dynamics model, SDM, oscillating in both pitch and plunge modes. Up to now, there has been little or no result on the plunging behavior of an aircraft or missile as a whole and the present experiments can be considered as one of the first attempts to study the compressible flow field over a model undergoing both pitching and plunging motions. The experiments involved measuring normal force and pitching moment of the model at Mach numbers of 0.4, 0.6 and 1.5 and oscillation frequencies of 1.25, 2.77 and 6.00 Hz. The longitudinal dynamic derivatives were then calculated from the measured data. The pitching results have been compared with the available data on the same model and good agreement has been achieved. However no plunging data on the same or a similar model was available in the literature to be compared with the present findings.

Keywords– Pitching motion, plunging motion, hysteresis loop, stability derivative, pitch damping derivative

1. INTRODUCTION

The trend toward increased maneuverability and higher angles of attack in aircraft and missile design has compounded difficulties involved in dynamic stability predictions. Unsteady aerodynamic effects in general have a major impact on maneuverability and controllability of an aircraft [1]. In a longitudinal plane, the aircraft can perform a pure sinusoidal pitching maneuver as shown in Fig. 1a, where the aircraft instantaneous angle of attack remains constant and the pitch attitude changes sinusoidally. During a pure sinusoidal plunging motion, the pitch attitude is preserved and the instantaneous angle of attack changes sinusoidally due to the induced velocity effects, Fig. 1b. However, in a sinusoidal oscillation about a fixed axis, as shown in Fig. 1c, both pitch attitude and instantaneous angle of attack can be expressed as a function of both time and the angular velocity.

In an oscillatory motion the element of time makes the flow pattern more complicated. During pitch oscillation, the forebody vortices change their lateral and a vertical position as functions of the angle of attack, which itself is a function of time. Similarly, leading edge vortices periodically vary their longitudinal location at which they burst. Various components of the aircraft, such as fins and a horizontal tail, move in and out of the local flow regions in which they are embedded. These local flow motions are not simultaneous with the aircraft motion, but with a certain delay mainly due to the convective time lag, which is a function of the distance between the station under consideration and the station at which a particular flow phenomenon originates. This delay is mainly due to the fluid inertia and can be considered

*Received by the editors October 23, 2005; final revised form January 2, 2007.
**Corresponding author

as the main source of hysteresis loops observed in the force and moment variations with the angle of attack for a vehicle in an oscillatory motion [2].

(a) Pure pitching motion, q=sinωt, $\dot{\alpha} = 0$

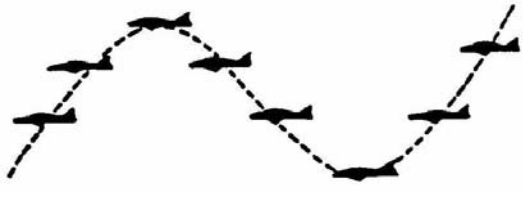

(b) Pure plunging motion, q=0, $\dot{\alpha} = \sin \omega t$

(c) Combination of pitching and plunging motions $q = \dot{\alpha} = \sin \omega t$

Fig. 1. Illustration of sinusoidal oscillatory motions for an aircraft

This phenomenon has been illustrated in Fig. 2 for a 70° swept wing at high incidence [3]. According to this figure, the flowfield over the wing surface differs during upstroke and downstroke motions when compared to the static case at the same angle of attack. As a result, the normal force will have different values during upstroke and down stroke motions, thus a hysteresis loop in the normal force is formed.

a) Upstroke motion

b) Downstroke motion

c) Static Case

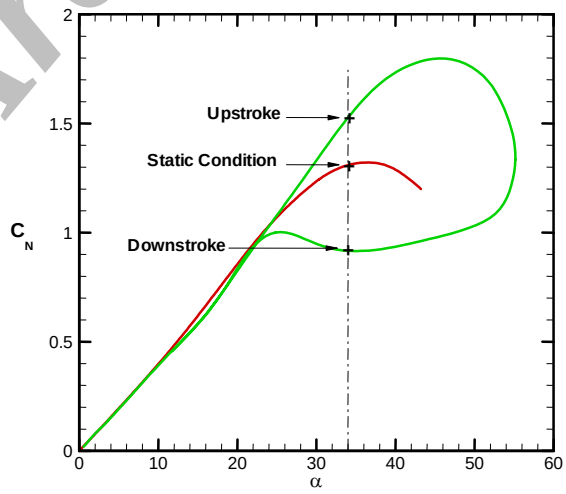

d) Different values for C_N and hysteresis loop formation

Fig. 2. Different flowfield in upstroke and downstroke motions and the hysteresis loop mechanism for a 70° delta wing [3]

The flow mechanisms responsible for these unsteady effects are the dynamic lag of the vortex bursting and flow separation phenomenon. Investigations have shown that the hysteresis loops observed in aerodynamic forces and moments depend on the amplitude, reduced frequency and the mean angle of attack of the oscillations. When the model oscillates at high angles of attack, the hysteresis loops widen and as the oscillation frequency increases, the size of these hysteresis loops is also increased.

In an oscillatory pitching motion, the aircraft is rotating about a spanwise axis and for most cases, through the center of gravity. Both the wing and the tail are affected by the rotation. Although, when the aircraft has a tail, the wing contribution to C_L and C_m due to pitch rate is negligible in comparison with that of the tail for most cases. The pitching moment has a generally large pitch rate dependency since the tail force, having a large moment arm, is a major contributor to the aircraft pitching moment. In contrast, the lift has a weaker dependency to the pitch rate because the tail force is just a small part of the total lift of an aircraft.

Numerous studies have documented the unsteady aerodynamic behavior of aircraft and missiles undergoing pitch oscillations, especially at high angles of attack [1-7]. However few works have been devoted to studying the aerodynamic behavior of flying vehicles undergoing a plunging motion.

An understanding of the complex flow mechanisms and the corresponding aerodynamic loads of a 3D configuration under transient plunging motion is, therefore, an important gap in our knowledge of the unsteady problems. Further, this information, along with that of sinusoidal pitching at the same reduced frequencies and Mach and Reynolds numbers, can be used to distinguish the effects of angle of attack, pitching velocity, $\dot{\alpha}$ and q. The intention of the current research work is to examine the flow field and the associated force and moment characteristics of a standard dynamics model undergoing a plunging motion at different Mach numbers, frequencies, mean angles of attack, etc.

In this paper, the aerodynamic loads on the model undergoing both pitching and plunging motions at various conditions are presented. The model was a standard dynamics model known as SDM. Static and dynamic normal force and pitching moment were measured using a 5-component internal strain gauge balance located inside the model. The experiments were conducted at Mach numbers of 0.4, 0.6 and 1.5 corresponding to Reynolds numbers of 0.84, 1.26 and 3.15×10^7 per meter, respectively. Dynamic data were taken at various combinations of reduced frequencies, mean angles of attack and oscillation amplitudes for the plunging motion. All tests have been conducted at zero sideslip angle.

2. MODEL AND EXPERIMENTAL APPARATUS

The model considered in the present experiments was typical of a fighter aircraft called the standard dynamics model (SDM) and has been used in many research centers for flow field study and verification of dynamic test rigs for several years all over the world [4-7]. It is a simplified model of the F-16 aircraft. The SDM manufactured for the present experiments has a 32 cm length and 10.34 cm semi span. This model is shown in Fig. 3.

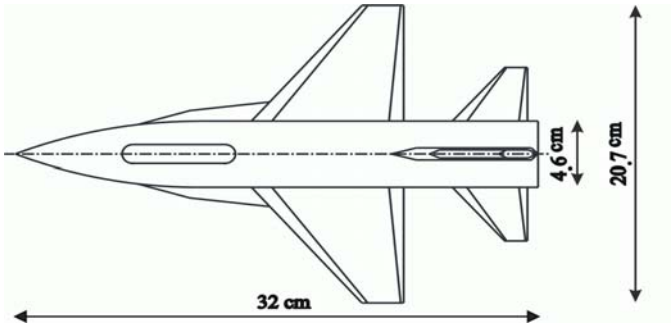

Fig. 3. Schematic view of SDM constructed for the present experiments

The model was tested in the trisonic wind tunnel of the aerodynamic lab at IHU, Iran. It is a continuous open circuit tunnel with test section dimensions of 60×60×120 cm^3. The test section Mach number varies from 0.4 to 2.2 via the engine RPM and different nozzle settings. Static and direct derivatives in pitch and plunge modes at various frequencies, Mach numbers and mean angles of attack were measured [8].

The oscillatory pitching data were taken at oscillation amplitudes of ±1 and ±5 degrees and frequencies of 1.25, 2.77 and 6.00 Hz. For the plunging maneuver, the mean angles of attack were 0, 6 and 12 degrees and the heaving amplitudes ±1, ±3 and ±5 cm with the same oscillation frequencies as those of the pitching case.

Dynamic oscillatory data presented here are an average of several cycles at a sample rate based on the oscillation frequency. Various data acquisition rates were examined to find the best combination to provide as many cycles of quality data as possible. Raw data were then digitally filtered using a low-pass filtering routine. During the filtering process, cut off and transition frequencies were varied until the deviation between the original and the filtered data was at a minimum. A sample filtered data from the potentiometer during a pitching motion of the model has been shown in Fig. 4. Due to the misalignments and manufacturing tolerances in the oscillation system and the connecting rods, the hysteresis loops did not repeat themselves exactly in each oscillation cycle. In order to have a clearer view of the loops and to increase the calculation accuracy, the filtered data presented in this paper have been averaged over at least 5 cycles of oscillation [9]. Figure 5 shows the averaged hysteresis loop of the normal force for a sample case.

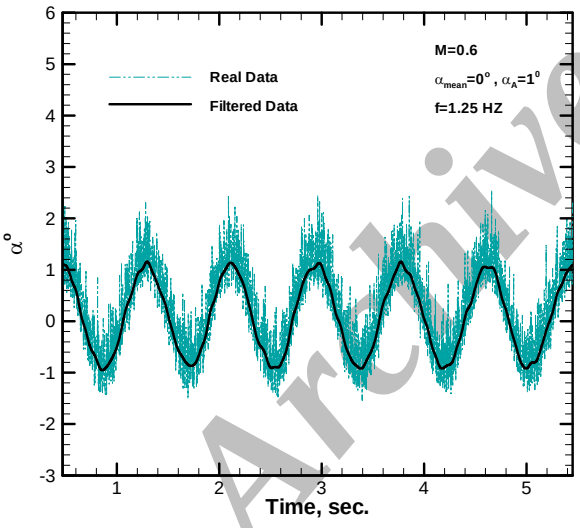

Fig. 4. Comparison of the filtered and raw data for a sample case

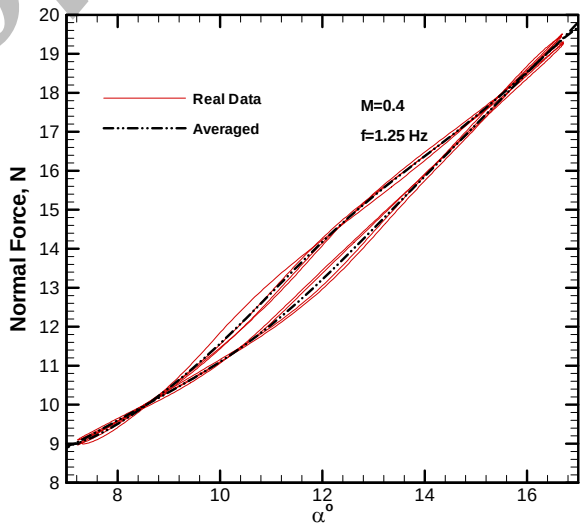

Fig. 5. Data averaging over the five mid cycles for the normal force

The model was oscillated to about 35% of its mean aerodynamic chord and the aerodynamic moment derivatives in the present paper were calculated about this point. The inertial force and moment were measured at the wind-off condition at the same oscillation frequencies as the wind-on runs. The magnitude of the tares was then subtracted from the values recorded in the wind-on runs.

3. RESULTS AND DISCUSSION

Figure 6 shows the variations of the dynamic normal force and pitching moment coefficients with angle of attack for three different reduced frequencies, two mean angles of attack; α_{mean}=0 and 14 degrees and at a

constant Mach number of 0.6. Static data for all cases are also shown for comparison. From this figure, it is seen that as the reduced frequency increases, both the slope and width of the hysteresis loops decreases.

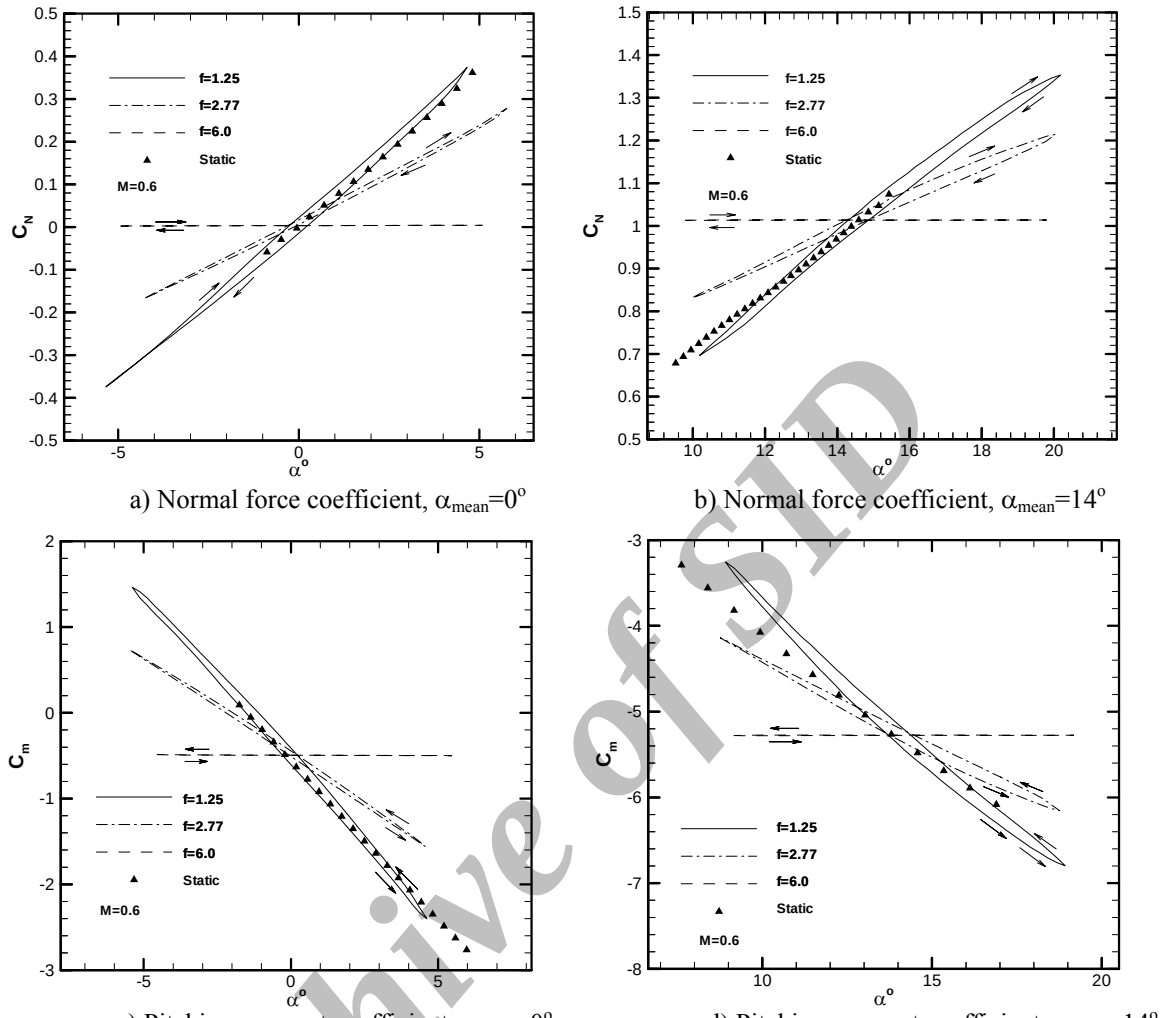

a) Normal force coefficient, $\alpha_{mean}=0^o$ b) Normal force coefficient, $\alpha_{mean}=14^o$

c) Pitching moment coefficient, $\alpha_{mean}=0^o$ d) Pitching moment coefficient, $\alpha_{mean}=14^o$

Fig. 6. Variations of longitudinal force and moment with angle of attack in pitching motion

From Fig. 6 note that the values of C_N and C_m at any instantaneous angle of attack between the upstroke and downstroke motion is different, indicating a time lag in the flowfield over the model. In such an unsteady motion, the difference between the motion of the model and the corresponding flowfield around it at any instantaneous angle of attack creates the hysteresis loop in both C_N and C_m data. In a certain frequency range, as the oscillation frequency increases, the phase difference between the motion and the corresponding flow around the model decreases. Thus the width and slope of the hysteresis loop is decreased. At f=6.00 Hz, the flow no longer follows the motion of the model. Consequently the upstroke and downstroke curves collapse on each other and C_N and C_m will have a nearly constant value for the range of angle of attack tested [9]. Further, note that for zero degree mean angle of attack, the static data for both C_N and C_m fall within the dynamic values at the frequency of 1.25 Hz in Figs. 6a and 6c, but for the mean angle of attack of 14 degrees, the situation differs, especially for the C_m case as seen from Fig. 6d. This phenomenon is mainly due to the strake vortices and the effects of oscillation frequency on their development, breakdown, etc.

From this figure, the effects of the mean angle of attack on the dynamic and static variation of the longitudinal force and moment of the SDM are clearly seen. As the mean angle of attack increases from 0

to 14 degrees, the variations mentioned before become nonlinear, which are indications of the strake vortices formation, and their breakdown and flow separation over the wing and tail surfaces.

Figure 7 shows variations of the vertical displacement and the corresponding induced angle of attack due to the plunging motion of the model with time at a frequency of 1.25 Hz. As the plunging amplitude increases, values of the induced angle of attack increase too. For all amplitudes shown here, the motion was around zero degree mean angle of attack and varied sinusoidally with time at different frequencies, amplitudes, etc. The corresponding induced angle of attack, which is due to the oscillation time history effects on the vertical motion of the model, is also sinusoidal as shown in this figure. However since the free stream velocity is relatively high (the lowest Mach number tested was 0.4), the variation of the resulting induced angle of attack is small, about ±0.125 degrees for the extreme case, i.e. the plunging amplitude of H_A=±5 cm and frequency of 6.00 Hz. For higher plunging frequencies, these values are higher. In order to get higher induced angles of attack, the plunging amplitudes must be increased, which is restricted by the tunnel test section size (60 ×60 cm^2), and the free stream velocity must be lowered significantly or the model should be plunged at higher frequencies. The latter is limited by the balance strength due to high aerodynamic and inertial loads and the plunging mechanisms.

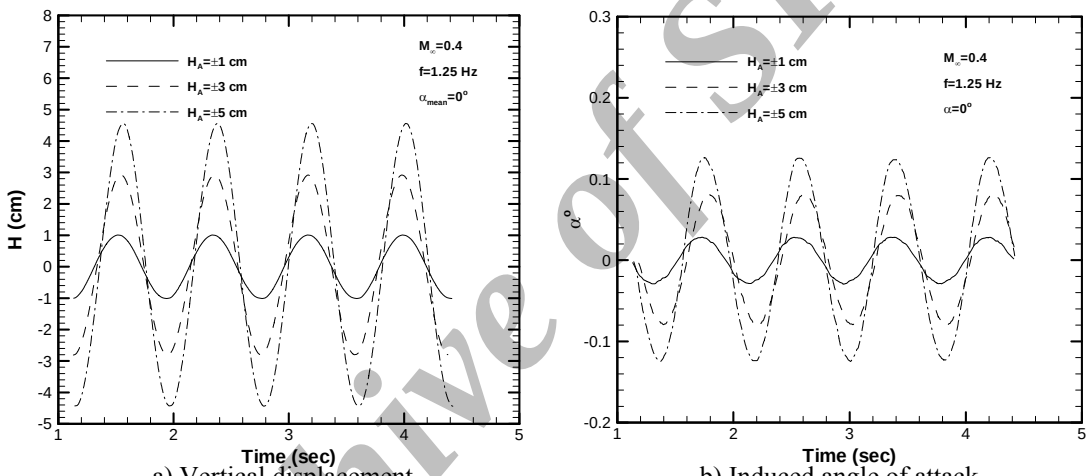

a) Vertical displacement b) Induced angle of attack

Fig. 7. Time variations of parameters in a plunging motion

Variations of vertical displacement of the model with an induced angle of attack during plunging motion for a Mach number of 0.4 and zero degree mean angle of attack are shown in Fig. 8. For a constant plunging amplitude of ±5 cm, Fig. 8a illustrates that increasing the heaving frequency stretches the loops of the vertical displacement versus the induced angle of attack, with their tops and bottoms nearly coincided. Figure 8b shows that variations of the vertical displacement with the induced angle of attack form co-centric circles. The radius of the circles increases as the plunging amplitude increases. However from Fig. 8, it is seen that the effect of oscillation frequency on the induced angle of attack is more pronounced than that of the oscillation amplitude. This figure clearly illustrates that to increase the induced angle of attack it is more convenient to increase the plunging frequency than plunging the model at higher amplitudes.

Figure 9 shows the effects of plunging frequency on variations of the normal force coefficient with vertical displacement for three amplitudes of ±1, ±3 and ±5 cm and at a constant Mach number of 0.4. For both oscillation frequencies of 1.25 and 2.77 Hz, there exists a hysteresis loop between increasing (upstroke) and decreasing (downstroke) angles of attack, as observed earlier in the pitching data.

At a certain frequency range, depending on the geometry and free stream conditions, as the oscillation frequency increases, the phase difference between the motion and the corresponding flow around the model decreases. Thus the width and shape of the hysteresis loop varies. At *f*=6.00 Hz, however, the

upstroke and downstroke curves collapse on each other and C_N exhibits a nearly constant value for the range of the vertical displacements tested. This phenomenon has previously been observed in the pitching results too. However it seems that the different phase lags in the flow fields for f=1.25 and 2.77 Hz in the plunging motion have been justified by the long oscillation time history at an amplitude of ±5 cm shown in Fig. 9c. Consequently at this amplitude, the loops for f=1.25 Hz and f=2.77 Hz nearly collapse on each other.

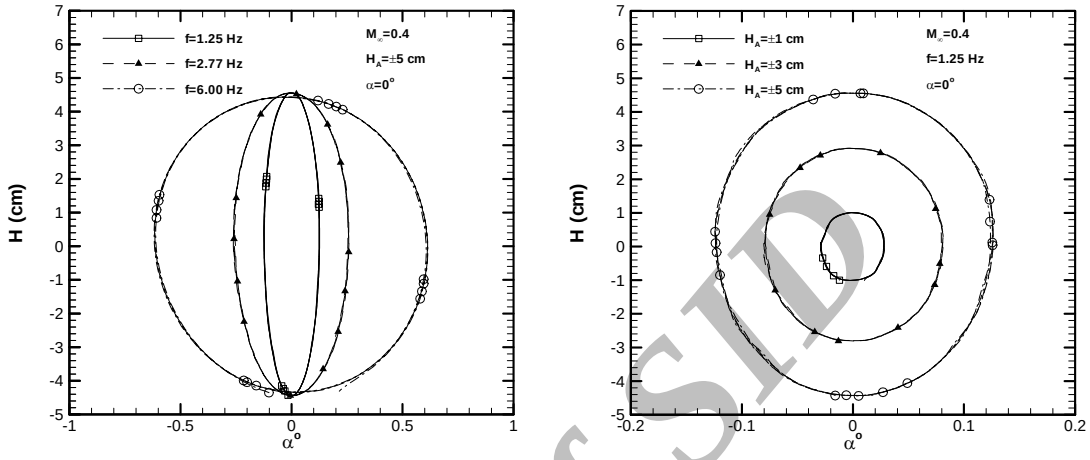

a) Effect of plunging frequency b) Effect of plunging amplitude

Fig. 8. Variations of vertical displacement with induced angle of attack

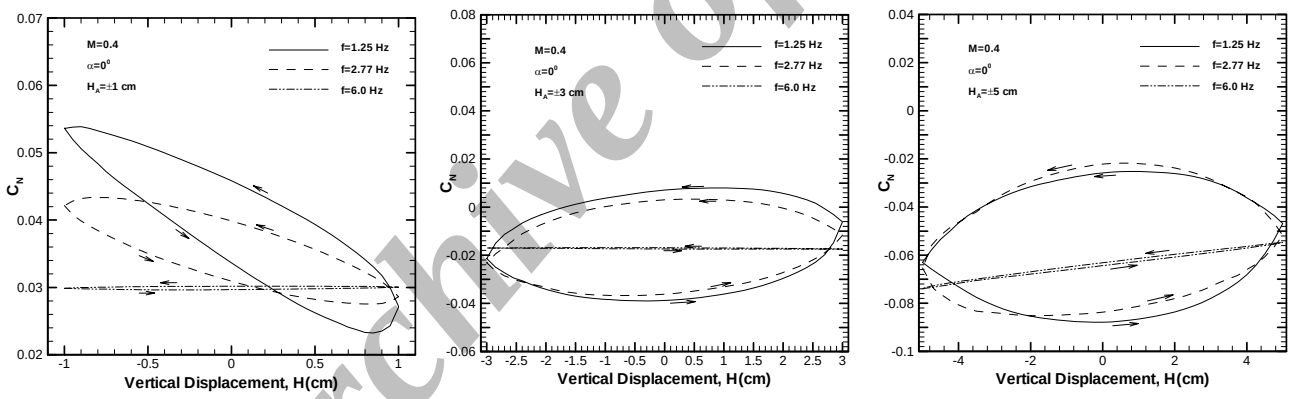

a) H_A=±1 cm b) H_A=±3 cm c) H_A=±5 cm

Fig. 9. Variations of the normal force coefficient with vertical displacement

For the lowest plunging amplitude tested here, H=±1 cm, Fig. 9a shows that the values of C_N are positive for all three plunging frequencies, f=1.25, 2.77 and 6.00 Hz. However as the plunging amplitude increases, the value of C_N for all frequencies becomes negative and decreases with increasing the heaving amplitude, H=±3 and ±5 cm as shown in Figs. 9b and 9c. Furthermore, figure 9 shows that for the lowest amplitude, the normal force coefficient for the plunging frequency of 1.25 Hz is higher than the corresponding values for f=2.77 Hz for all angles of attack. However, as the plunging amplitude increases, these differences decrease and the hysteresis loops for both frequencies become almost identical (Fig. 9b), but the absolute value of C_N for the plunging amplitude of 1.25 Hz is still slightly higher. By further increasing the plunging amplitude, H=±5 cm, Fig. 9c shows that the differences in the C_N values for the heaving frequencies of 1.25 and 2.77 Hz almost vanish.

Effects of oscillation amplitude on the variations of the normal force coefficient at a Mach number of 0.4, plunging frequency of 1.25 Hz and two different mean angles of attack of 0 and 12 degrees are shown in Fig. 10. As the amplitude increases, the values of the normal force coefficient for all angles of attack

decrease, the corresponding hysteresis loop becomes more symmetric, and its width also increases. Similar trends are observed when the mean angle of attack is increased to 12 degrees (Fig. 10b). Higher values of C_N, seen in this figure for all plunging amplitudes, is due to the mean angle of attack of 12 degrees. However it seems that plunging about a higher mean angle of attack reduces the width of the hysteresis loop.

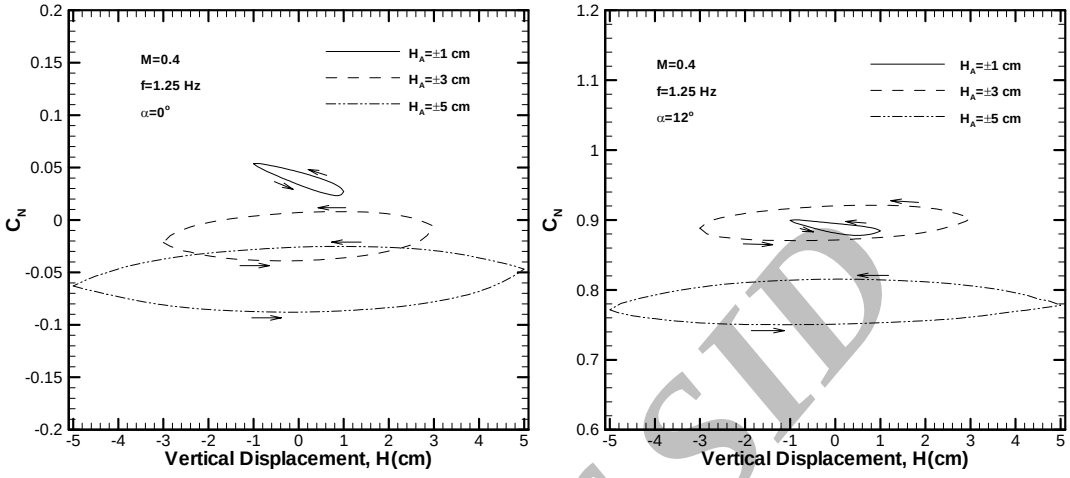

a) $\alpha_{mean}=0^o$ b) $\alpha_{mean}=12^o$

Fig. 10. Effects of plunging amplitude on variations of the normal force coefficient with vertical displacement

Figure 11 shows the effects of oscillation frequency on the variations of C_N for two Mach numbers of 0.6 and 1.5, two mean angles of attack of 0 and 12 degrees and a plunging amplitude of ±3 cm. Note that the variations with frequency for both mean angles at M=0.6 have nearly the same trend but different values. For a mean angle of attack of 12 degrees, Fig. 11c, C_N has higher values for all instantaneous vertical positions when compared with Fig. 11a. Further inspecting Figs. 11a and 11c, it seems that plunging about higher mean angles of attack reduces the width of the hysteresis loop for all angles of attack, a phenomenon which was seen previously in Fig. 10. For a Mach number of 1.5, Figs. 11b and 11d show that not only the width of the hysteresis loops have changed when the mean angle of attack increased from 0 to 12 degrees, but also their shape altered too. Figure 11d indicates that the values of C_N for f=2.77 Hz are higher than the corresponding values for the case of f=1.25 Hz. The most important aspect of Fig. 11 is the direction of the hysteresis loops, which has been reversed in supersonic flow compared to the corresponding loops at the subsonic Mach number of 0.6.

Figure 12 shows the variations of C_N for two different mean angles of attack of 0 and 12 degrees, plunging frequency of 1.25 Hz and plunging amplitude of ±5 cm. The value of C_N at M=0.6 is higher than the corresponding value at M=0.4. This sharp increase in C_N when the model is plunged at a mean angle of attack of 12 degrees is probably caused by transonic effects. At this angle of attack it is more likely that the flow over a portion of the upper surface of the model is supersonic, thus reducing the local pressure and creating higher normal force coefficients. The drop in C_N for M=1.5 is probably due to the shock system developed on the body and the shock induced separation phenomenon on the rear part of the cockpit. Note that the hysteresis loops for subsonic Mach numbers are counterclockwise, while those of the supersonic case are clockwise. Further, as seen before, for all cases presented in Fig. 12, variation of C_N with the vertical displacement is almost symmetric and similar with each other for all Mach numbers tested.

The dynamic derivatives in the present experiments were calculated from the normal force and pitching moment data. Both motions were sinusoidal in the form of $\alpha(t)= \alpha_A \sin[2\pi ft]$ in pitching and $H(t)=H_A \sin[2\pi ft]$ in plunging motions. So, the in-phase and the out of phase derivatives represent sine and

cosine Fourier coefficients, respectively. The longitudinal dynamic derivatives were then calculated by the Fourier integral of the pure dynamic normal force and pitching moment over 5 oscillation cycles.

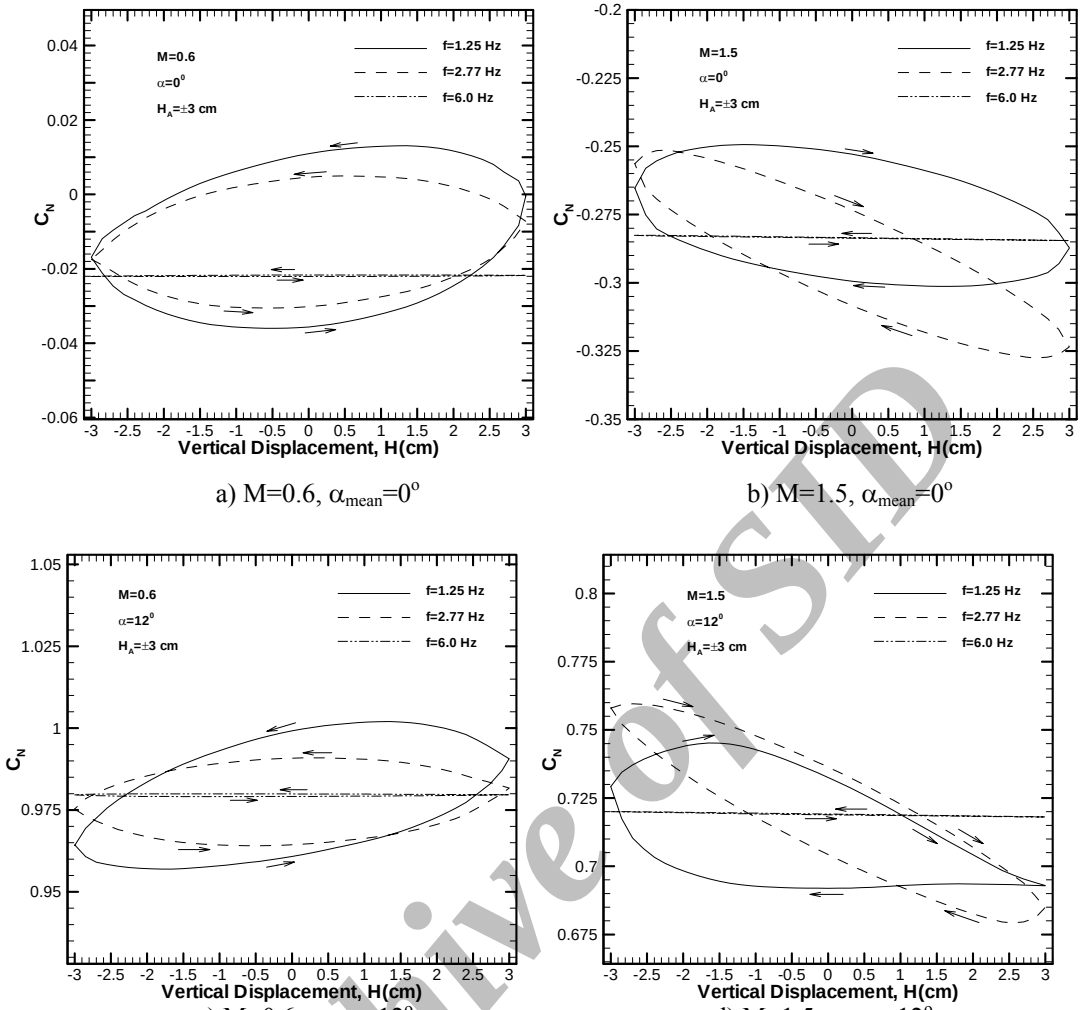

a) M=0.6, $\alpha_{mean}=0^o$ b) M=1.5, $\alpha_{mean}=0^o$

c) M=0.6, $\alpha_{mean}=12^o$ d) M=1.5, $\alpha_{mean}=12^o$

Fig. 11. Effects of plunging frequency on variations of the normal force coefficient with vertical displacement

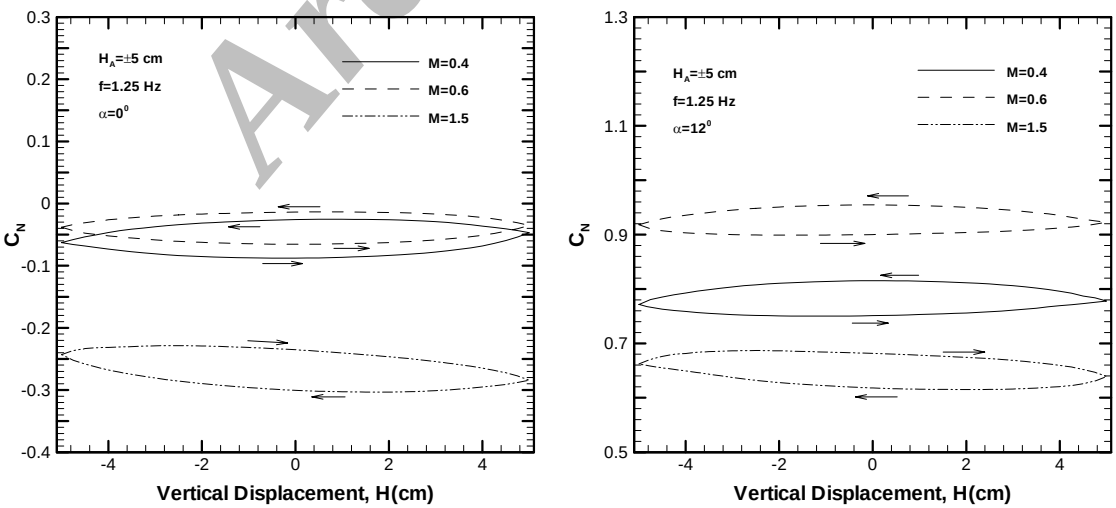

(a) $\alpha_{mean}=0^o$ (b) $\alpha_{mean}=12^o$

Fig. 12. Effects of Mach number on variations of the normal force coefficient with vertical displacement

Figure 13 shows variations of the normal force slope and pitch damping coefficients with an angle of attack for a subsonic Mach number of 0.6. It should be noted that the present tunnel setup and the alpha-mechanism system used for changing the angle of attack of the model for both static and dynamic studies were such that the maximum static angle of attack obtainable in the test section for this particular model was about 18°. In addition, the blockage problem in dynamic tests necessitated this angle of attack limitation [9].

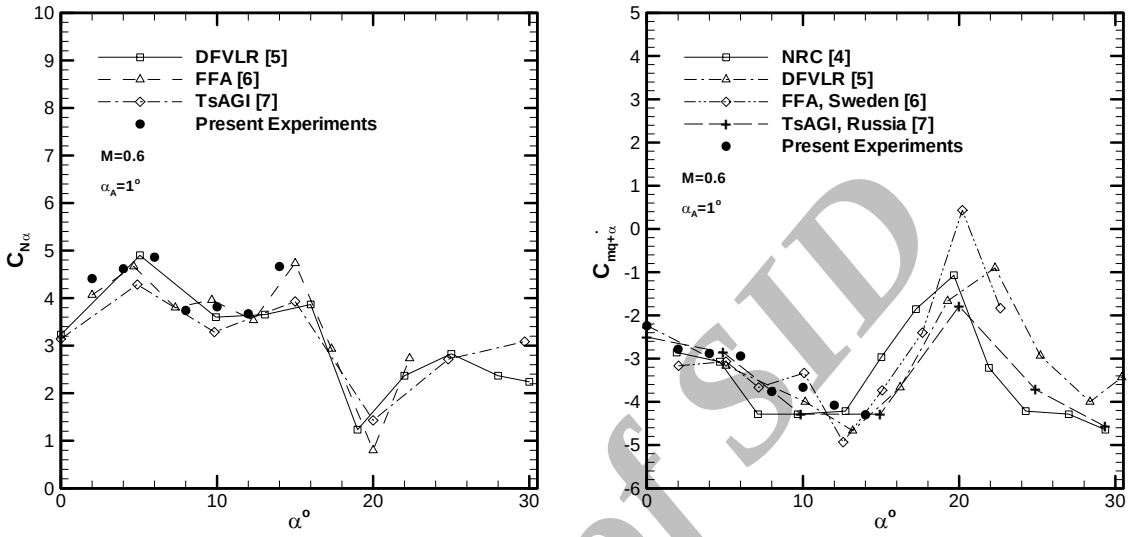

a) $C_{N\alpha}$ b) $C_{m_{q+\dot{\alpha}}}$

Fig. 13. Variations of the dynamic pitching derivatives with mean angle of attack

The present results are compared to the previously obtained dynamic database for this model [4-7], and as seen from Fig. 13, good agreements are achieved verifying the accuracy of the measured parameters. This comparison also indicates that the experimental set up as well as the data acquisition system, data corrections and reduction schemes are correct. From Fig. 13a note that $C_{N\alpha}$ first reaches its maximum value at about a 5° angle of attack. Beyond this angle, $C_{N\alpha}$ decreases drastically indicating flow separation over the wing surface. The normal force slope continues to decrease until an angle of attack of about 10°. By further increasing the angle of attack, $C_{N\alpha}$, starts to increase again. The experimental data [10] indicate that for a delta wing with a leading edge sweep of about 70° the leading edge vortices start to form at an angle of attack of about 10°, causing a nonlinear increase in the normal force data. These vortices create additional lift, known as vortex lift. The present model has strakes with a leading edge sweep of about 73°. Thus the increase in $C_{N\alpha}$ at angles of attack beyond 10° shown in Fig. 13a is due to the formation of the strake vortices. From this figure it is seen that $C_{N\alpha}$ increases until an angle of attack of about 15°. This increase in $C_{N\alpha}$ is due to the strength of the strake vortices even though the flow over the main portion of the wing is separated. Subsonic flowfield study over a wing surface of a similar model indicated that the maximum lift occurs at about a 12 degree angle of attack [11]. Beyond this angle of attack, separated flow is dominant over the main portion of the wing surface, deteriorating the aerodynamic performance. As mentioned before, the present experimental setup was limited to a mean angle of attack of about 18°. However variations of $C_{N\alpha}$ with α for the range of angles of attack tested compare well with those of Ref. [4-7].

Figure 13b compares variations of the present pitch damping derivative result with other findings. Again within the range of the angles of attack tested, the data compares well with those of Ref. [4-7]. From this figure, it is seen that the pitch damping derivative continuously decreases as the angle of attack is increased, a dynamically stable condition. Beyond an angle of attack of 15 degrees, the reduction of

dynamic stability is due to the strake vortices breakdown location which has reached the tail surfaces, hence decreasing the stability level.

Figure 14 shows variations of the normal force slope with mean angle of attack for the plunging motion of SDM. The values for the pitching case are also included for comparison. According to Fig. 14, the plunging values of $C_{N\alpha}$ are much higher than the pitching ones. Note that in the present experiments the value of the induced angle of attack during a plunging motion is much smaller than the geometric angle of attack in its corresponding pitching motion. As a result, the dynamic normal force slope, $C_{N\alpha}$, for a plunging motion is higher than that in a pitching motion. However the plunging motion in the present experiments has been conducted at three mean angles of attack of zero, 6 and 12 degrees. So an exact survey on the trend of the plunging $C_{N\alpha}$ for different mean angles of attack is not possible from Fig. 14.

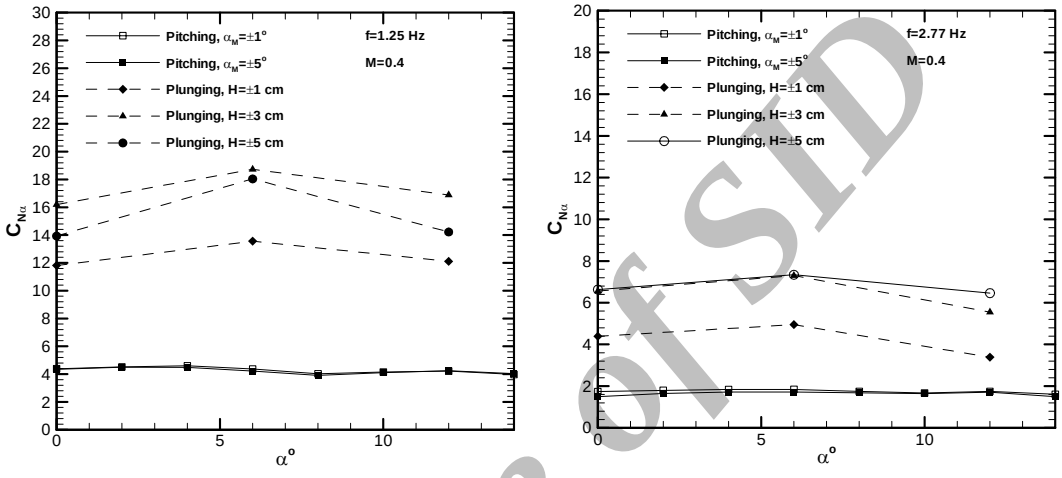

a) f=1.25 Hz b) f=2.77 Hz

Fig. 14. Variations of dynamic $C_{N\alpha}$ with mean angle of attack

Figure 15 compares the normal force damping derivatives in pitching and plunging motions for M=0.4, two oscillation frequencies of 1.25 and 2.77 Hz, and from Fig. 15a it is evident that for the frequency of 1.25 Hz, $C_{N_{\dot\alpha}}$ is nearly one half of $C_{N_{q+\dot\alpha}}$. Since $C_{N_{\dot\alpha}}$ strongly depends on $\dot\alpha$ and $C_{N_{q+\dot\alpha}}$ is a function of the term $q+\dot\alpha$, it can be concluded that almost half of the normal force damping derivative, $C_{N_{q+\dot\alpha}}$, is due to $\dot\alpha$, hence the remainder will be the contribution of pure pitching derivative C_{Nq}.

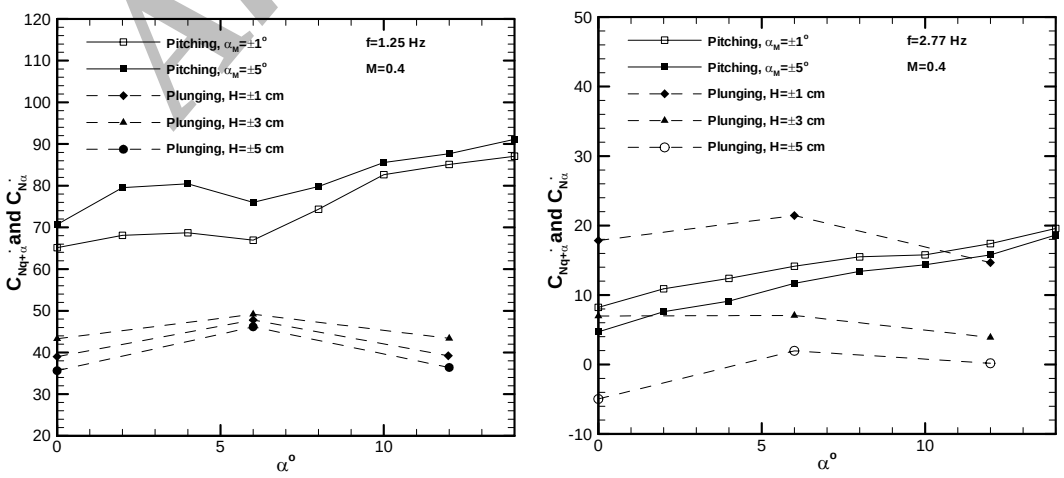

a) f=1.25 Hz b) f=2.77 Hz

Fig. 15. Variations of dynamic $C_{N_{q+\dot\alpha}}$ and $C_{N_{\dot\alpha}}$ with mean angle of attack

As the oscillation frequency increases, both the pitch rate, q, and the time rate of change of the induced angle of attack, $\dot{\alpha}$, increase (see the definitions of q and $\dot{\alpha}$). Further, note that they are both directly proportional to f. Since $C_{N_{\dot{\alpha}}}$ and $C_{N_{q+\dot{\alpha}}}$ are differentiated with respect to $\dot{\alpha}$ and q, at higher frequencies, and since these two independent variables increase, the derivatives $C_{N_{\dot{\alpha}}}$ and $C_{N_{q+\dot{\alpha}}}$ decrease. This can be seen from Fig. 15b for f=2.77 Hz. However q is a stronger function of the frequency, thus the rate of decrease of $C_{N_{q+\dot{\alpha}}}$ would be steeper than $C_{N_{\dot{\alpha}}}$. Contrary to the case of f=1.25 Hz in Fig. 15a, for the frequency of 2.77 Hz, the values of $C_{N_{\dot{\alpha}}}$ and $C_{N_{q+\dot{\alpha}}}$ are of the same order, hence C_{Nq} has a very small contribution to the normal force damping derivative.

On the other hand, the dynamic lift in an unsteady motion can be expressed as the sum of the oscillatory lift and the apparent mass effects. The increase in $C_{N_{\dot{\alpha}}}$ in the present experiments is mainly due to the apparent mass effects that dominate the circulatory lift at high oscillation frequencies [12]. Note that C_{Nq} is mainly due to the flow upwash and downwash effect, while $C_{N_{\dot{\alpha}}}$ is due to variations of the effective angle of attack. At higher oscillation frequencies the upwash and downwash effects almost diminish, which means that the flow cannot follow the motion as it did at lower frequencies. This phenomenon is probably the main reason for decreasing the dynamic $C_{N\alpha}$ at higher frequencies as observed in Figs. 6, 9 and 11.

A similar trend can be observed in the pitch damping derivative behavior shown in Fig. 16. According to Figs. 16a and b for both frequencies, the model is dynamically unstable during a plunging motion, while for pitching motion it is stable throughout the mean angles of attack tested. As noted earlier, in high speed flow, as was the case for the present experiments, $\dot{\alpha} = \dot{H}(t)/V_\infty$ for a plunging motion is usually smaller than $q = c\omega/2V_\infty$ for the pitching motion for the same oscillation frequencies. Thus the absolute value of $C_{m_{\dot{\alpha}}}$ is smaller than $C_{m_{q+\dot{\alpha}}}$ in the present experiments.

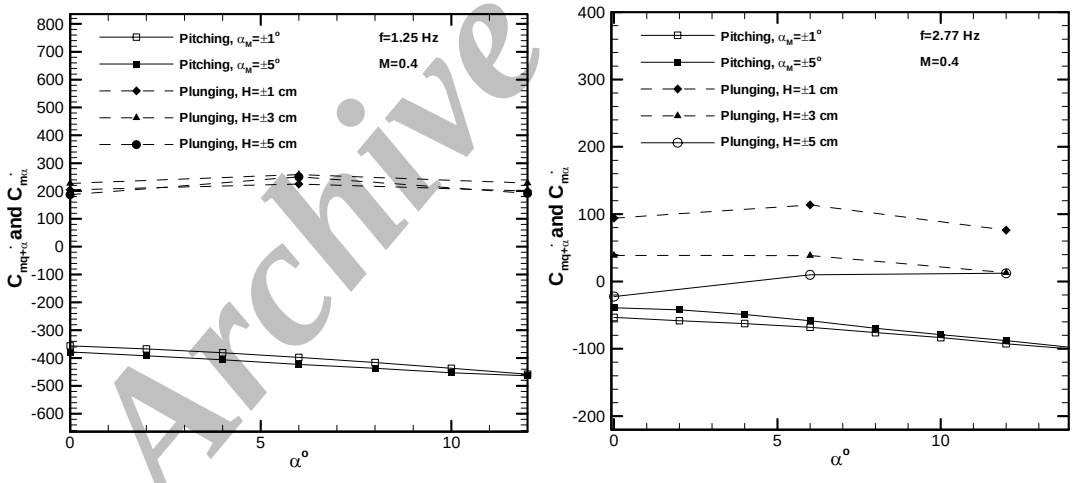

a) f=1.25 Hz b) f=2.77 Hz

Fig. 16. Variations of dynamic $C_{m_{q+\dot{\alpha}}}$ and $C_{m_{\dot{\alpha}}}$ with mean angle of attack

Figure 16b shows that as the oscillation frequency increases, the absolute values of both dynamic derivatives in pitch and plunge modes decreases. In other words, increasing the oscillation frequency decreases the dynamic stability for both pitching and plunging motions. However, the difference between $C_{m_{q+\dot{\alpha}}}$ and $C_{m_{\dot{\alpha}}}$ determines the pure pitch damping contribution, C_{m_q}. As is seen, C_{m_q} is negative and its effect is to increase the damping characteristics of the model. This can improve the dynamic stability attitude of the model.

Figure 17 shows the effects of the Mach number on variations of the plunging derivatives; $C_{N\alpha}$, $C_{m\alpha}$, $C_{N_{\dot{\alpha}}}$ and $C_{m_{\dot{\alpha}}}$ with mean angle of attack. According to Fig. 17a, in the subsonic regime, dynamic $C_{N\alpha}$ increases as the Mach number changes from 0.4 to 0.6. However in the supersonic regime, a dramatic drop

in $C_{N\alpha}$ is observed, which is an indication of the shock induced separation on the model. A similar trend is seen in the variations of the pitching moment slope with mean angle of attack shown in Fig. 17b. Effects of supersonic flow and unsteady shock waves have caused intense instability. Supersonic flow effect also has an impact on the models dynamic stability. Variations of $C_{N_{\dot{\alpha}}}$ and $C_{m_{\dot{\alpha}}}$ with the Mach number shown in Figs. 17c and d shows a jump in these derivatives at M=1.5. Figure 17d shows that the model is dynamically unstable in the supersonic regime, while for both subsonic Mach numbers a neutral stability is observed. In the supersonic regime, due to the existence of shock waves, the flow field will be a strong function of the shock position and is less affected by the changes in the plunging-induced angle of attack. For this reason, the derivatives shown in Fig. 17 exhibit a different behavior in subsonic and supersonic regimes.

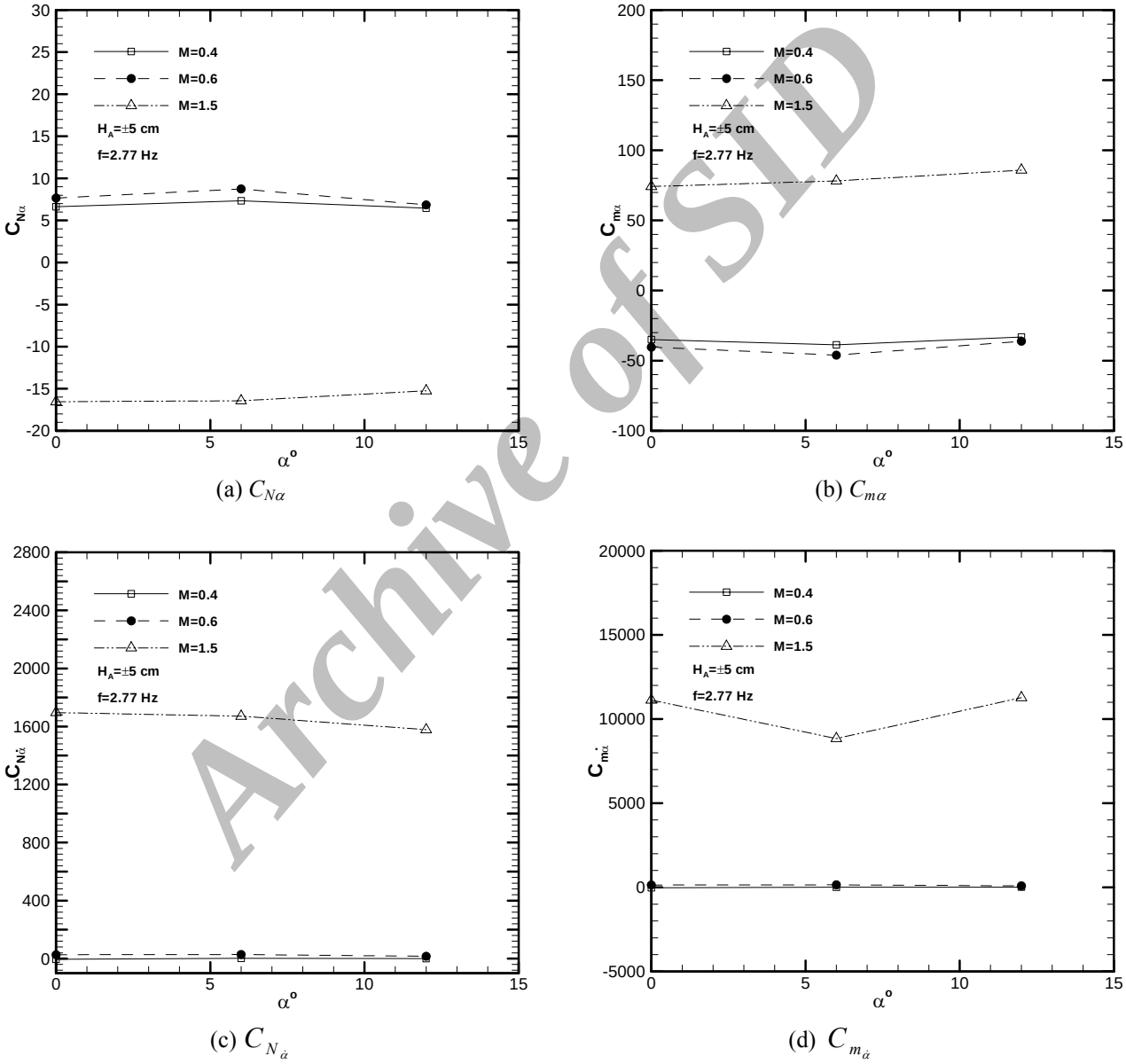

(a) $C_{N\alpha}$ (b) $C_{m\alpha}$

(c) $C_{N_{\dot{\alpha}}}$ (d) $C_{m_{\dot{\alpha}}}$

Fig. 17. Variations of the plunging derivatives with mean angle of attack

4. CONCLUSION

Extensive wind tunnel tests have been conducted to study the unsteady aerodynamic behavior of a standard dynamics model oscillating in pitch and plunge modes. The experiments involved measuring the

normal force and the pitching moment of the model for both motions. The dynamic derivatives were calculated using the acquired data. In a pitching motion, the pitching angular velocity, q, and the time rate of change of the angle of attack, $\dot{\alpha}$, determine the aerodynamic behavior of the oscillating body, while in a plunging motion there is no pitch rate and the only parameter determining the stability behavior of the model is $\dot{\alpha}$. Note that in the Mach number range tested here, the vertical velocity of the model was small compared to the free stream Mach number, hence the resulting induced angle of attack is too small. The results show that for both pitching and plunging motions, the width of the loop and slope of the normal force and pitching moment decreases as the frequency increases. In the plunging motion, the sensitivity of the aerodynamic force and moment to oscillation frequency was smaller than those of the pitching motion. As noted earlier, the vertical velocity during oscillation is negligible compared to the free stream velocity. So the induced angle of attack and hence the normal force due to the plunging motion is too small.

The results for static derivatives; $C_{N\alpha}$ and $C_{m\alpha}$, show that absolute values of the plunging $C_{N\alpha}$ and $C_{m\alpha}$ are higher than the pitching ones. This is because the induced angle of attack during a plunging motion is much smaller than the instantaneous geometric angle of attack in a corresponding pitching situation. The dynamic derivatives calculated in the present experiments are $C_{N_{q+\dot{\alpha}}}$ and $C_{m_{q+\dot{\alpha}}}$ for pitching motion and $C_{N_{\dot{\alpha}}}$ and $C_{m_{\dot{\alpha}}}$ for plunging motions. For a pitching motion, both q and $\dot{\alpha}$ are the contributor terms, but in a plunging motion, the only contributor is $\dot{\alpha}$. Hence the absolute values of the dynamic derivatives in a pitching motion, with respect to both q and $\dot{\alpha}$, are larger than the plunging ones. As the oscillation frequency increases, both pitching and plunging derivatives decrease, but since the pitching derivatives have a larger dependency on frequency, they have a steeper rate of decrease.

NOMENCLATURE

U	free stream velocity, m/sec	H_A	plunging oscillation amplitude, cm
M	free stream Mach number	C_N	normal force coefficient
C	wing mean aerodynamic chord, m	C_m	pitching moment coefficient
S_{ref}	wing area, m^2	$C_{N\alpha}$	dynamic normal force slope, /rad
f	oscillation frequency, Hz	$C_{m_{q+\dot{\alpha}}} = \frac{\partial C_m}{\partial\left[\frac{cq}{2U}\right]}$	pitch damping derivative, /rad
$q=2\pi f$	the pitching velocity, rad/sec		
A	instantaneous angle of attack, deg		
α_A	pitching oscillation amplitude, deg		
H	instantaneous vertical displacement in plunging motion, cm		
$\dot{\alpha} = \dot{H}/U$	plunging-induced angle of attack, rad.		

REFERENCES

1. Beyers, M. E. (1975). Free flight investigation of high-maneuverability missile dynamic. *Journal of Spacecraft and Rockets, 14*(4), 224-230
2. Orlik-Rückeman, K. J. (1983). Aerodynamic aspects of aircraft dynamics at high angles of attack. *Journal of Aircraft*, *20*(9), 737-751
3. Soltani, M. R. (1992). An experimental study of the relationship between forces and moments and vortex breakdown on a pitching delta wing. Ph.D. Thesis, University of Illinois at Urbana-Champaign.
4. Beyers, M. E. (1985). SDM Pitch and Yaw axis stability derivatives. *AIAA Paper*, 85-1827.
5. Schmidt, E. (1985). Standard dynamics model experiments with the DFVLR/AVA transonic derivative balance. *AGARD CP*-386.

6. Jansson, T. & Torngren, L. (1985). New dynamic testing techniques and related results at FFA. *AGARD CP*-386.
7. Kabin, S. V., Kolinko, K. A., Khrabrov, A. N. & Nushtaev, P. D. (1995). Dynamic test rig and test techniques for the aircraft models unsteady aerodynamic characteristics measurements n high subsonic and transonic wind tunnels. *Proceedings of IEEE International Congress on Instrumentation in Aerospace Simulation Facilities*, *ICIASF*, CH3482.
8. Davari, A. R. & Soltani, M. R. (2005). Force and moment measurements on a fighter model in heaving motion. *AIAA Paper 2005-0238*.
9. Davari, A. R. (2005). Experimental investigation of the effects of compressibility and reduced frequency on aerodynamic behavior of a flying vehicle. Ph.D. Thesis, Department of Aerospace Engineering, Sharif University of Technology.
10. Wentz, W. H. (1963). Wind tunnel investigations of vortex break downs. Ph.D. Dissertation, University of Kansas, Lawrence.
11. Soltani, M. R. & Davari, A. R. (2004). Experimental investigation of the dynamic stability derivatives of a fighter model oscillating in Pitch. *ICAS 2004-2.10.2, 24th ICAS Congress*, Japan.
12. Katz, J. & Plotkins, A. (2001). *Low speed aerodynamics*. Second Edition, 369-386, Cambridge University Press.